Catalysis Science & Technology

PAPER

View Article Online
View Journal | View Issue

Cite this: *Catal. Sci. Technol.*, 2015, 5, 3416

Facile structure design based on C_3N_4 for mediator-free Z-scheme water splitting under visible light†

Guixia Zhao,‡ Xiubing Huang,‡ Federica Fina, Guan Zhang and John T. S. Irvine*

Received 13th March 2015,
Accepted 28th April 2015

DOI: 10.1039/c5cy00379b

www.rsc.org/catalysis

In this work, two photocatalysts (*i.e.*, C_3N_4 and WO_3) were successfully combined into a heterojunction structure by a facile hydrothermal method for mediator-free overall water splitting, analogous to the natural photosynthesis over a two-step photoexcitation Z-scheme system. Hydrogen and oxygen are evolved with a 2 : 1 ratio by irradiating the C_3N_4-WO_3 composites loaded with Pt under visible light ($\lambda > 420$ nm) without any redox mediator. Introducing reduced graphene oxide (rGO) into the C_3N_4-WO_3 composites enhances the water splitting efficiency. Through optimizing the mass ratio in the C_3N_4-WO_3 composites, rGO content, amount of loaded Pt and pH value of the reacting system, the highest H_2/O_2 evolution rates of 2.84 and 1.46 μmol h^{-1} can be obtained, with a quantum yield of 0.9%. Our findings demonstrate that the hydrothermal method is a promising strategy for constructing intimate heterostructures for Z-scheme water-splitting systems without using any redox mediator, and that rGO can be used to further enhance the performance in optimized conditions.

1. Introduction

With the increasing energy demand and concerns about environmental issues, hydrogen gas is considered as a promising fuel because it produces no carbon emission and other harmful by-products.[1] The artificial photosynthesis for hydrogen generation through water splitting under visible light is an important approach, among which, the powdered-type two-step photoexcitation system, *i.e.*, Z-scheme photocatalysis system, is the most similar to natural photosynthesis.[2–6] Normally, a Z-scheme system contains two photocatalysts (one for H_2 evolution, and the other for O_2 evolution) and usually an electron mediator, which transfers the electrons from the excited O_2 photocatalyst to the holes generated in the H_2 photocatalyst.[7]

It is suggested that electron transfer is the rate-determining process.[8] The commonly used electron mediators are ionic redox couples such as IO_3^-/I^-,[2,3,9] or Fe^{3+}/Fe^{2+}.[4,9,10] Compared with these ionic redox couples, the solid electron shuttle is more advanced for the recycle of the photocatalyst and cleaning of water. The challenges for the efficient H_2/O_2 evolution lie in the electron-accepting and -donating abilities of the mediator, which should retain a dynamic equilibrium and remain stable during reactions.[11] Furthermore, interface contact in the ternary system also plays an important role in maintaining continuous electron flow between the two photocatalysts. Considering the extremely high conductivity and specific surface area of graphene, it may be a good candidate as electron mediator for a Z-scheme system.[11] Besides, it is also challenging to choose appropriate photocatalysts for realizing the intimate physical interaction with graphene, the efficient charge carrier separation, the H_2/O_2 evolution on the H_2/O_2 photocatalysts and then finally preventing water formation due to the backward reaction of H_2 and O_2.[12,13] In Iwase *et al.*'s report,[11] it has been shown that photoreduced graphene oxide (PRGO) was able to function as a solid electron mediator for Z-scheme overall water splitting, where $SrTiO_3$:Rh was used as H_2 evolution photocatalyst, with 0.7 wt% Ru as co-catalyst, and $BiVO_4$ was used as O_2 evolution photocatalyst. The PRGO was synthesized by photoreduction, *i.e.*, irradiating the mixture of graphene oxide and the photocatalyst (Ru/$SrTiO_3$:Rh or $BiVO_4$) in the presence of methanol as electron donor. For the combined PRGO/$BiVO_4$ and Ru/$SrTiO_3$:Rh under pH 3.5, the H_2 evolution rate is *ca.* 8 μmol h^{-1}, while under neutral conditions, the performance is much lower, which is considered to be due to the poor physical interaction between PRGO/$BiVO_4$ and Ru/$SrTiO_3$:Rh under neutral conditions. In total, the reported Z-scheme based on PRGO is complicated in preparation as the noble metals (*i.e.*, Ru and Rh) are used as co-catalyst and dopant, respectively, and the

School of Chemistry, University of St Andrews, St Andrews, Fife, UK.
E-mail: jtsi@st-andrews.ac.uk; Fax: +44 (0)1334463808; Tel: +44 (0)1334463817

† Electronic supplementary information (ESI) available: H_2 evolution performance by C_3N_4-rGO composites with TEOA as sacrificial agent under visible light, rGO contents in different C_3N_4-rGO composites, and the mass spectra results using D_2O. See DOI: 10.1039/c5cy00379b

‡ These authors contributed equally to this work.

performance is dependent on the acidity. Although Sasaki *et al.*[8] reported the interparticle electron transfer without any electron mediator, the water splitting can only proceed efficiently by acidifying the aqueous solution to realize the effective contact through the aggregation of the two photocatalysts, $Ru/SrTiO_3$:Rh and $BiVO_4$. Thus, more sturdy contacts between the H_2/O_2 evolution phototcatalysts need to be found.

Since the introduction of graphitic carbon nitride (C_3N_4) into heterogeneous catalysis in 2006,[14,15] this yellow polymer consisting of tri-*s*-triazines interconnected *via* tertiary amines has attracted increasing interest in materials research especially in H_2-evolution photocatalysis under visible light.[16–18] The band gap of C_3N_4 is *ca.* 2.7 eV, with the CB and VB positions located at *ca.* −1.1 eV and *ca.* +1.6 eV *vs.* normal hydrogen electrode (NHE), respectively.[16,19] More importantly, the preparation of C_3N_4 is low cost since it only consists of two elements (C and N). For O_2-evolution photocatalysis from water, tungsten trioxide (WO_3) has been widely investigated because of its suitable bandgap, high electron mobility, abundance and low cost.[20]

Herein, we introduced a novel method to generate a close contact between C_3N_4 and WO_3 by the reaction of $Na_2WO_4 \cdot 2H_2O$ and C_3N_4 under hydrothermal conditions. To enhance the performance, rGO was also used to function as electron mediator. By calcining a mixture of rGO and melamine, the graphene layer was able to be homogeneously mixed with C_3N_4 layers. Then through the hydrothermal method, the C_3N_4-rGO composites were loaded with WO_3 particles, which function as O_2 evolution photocatalyst. It is demonstrated that the binary (in the case of no rGO) or ternary (in the case of containing rGO) composites were able to give out H_2 and O_2 under visible light irradiation ($\lambda > 420$ nm) with relatively high performance when loaded with Pt as co-catalyst, and an appropriate amount of rGO will enhance the performance.

2. Experimental section

Synthesis of C_3N_4-rGO composite and pure C_3N_4

Graphene oxide was synthesized according to the modified Hummers method as described in our previous work.[21] The as-prepared GO was then reduced by the hydrothermal method. 60 mg of GO was dissolved in 30 mL of H_2O by moderate sonication and the pH was adjusted to about 7 using NaOH solution before transferring into a Teflon-lined steel autoclave, which was heated in an oven at 140 °C for 18 h. The obtained rGO was collected and washed with distilled water and ethanol several times, and dried at 90 °C for 2 h. C_3N_4-rGO composites were obtained by calcining the mixtures of melamine and rGO with different mass ratios. These C_3N_4-rGO composites are noted as C_3N_4-rGO-*x*, where *x* represents the mass ratio of melamine to rGO during the synthesis process. For example, the composite C_3N_4-rGO-150 was prepared by calcining the mixture of 20 mg of rGO and 3000 mg of melamine at 500 °C for 3 h with a 5 °C min^{-1} increasing rate. Pure C_3N_4 was also obtained by calcining melamine at 500 °C for 3 h.

Synthesis of C_3N_4-rGO-WO_3 and C_3N_4-WO_3 composites

The ternary composites are noted as C_3N_4-rGO-*x*-WO_3 *m*–*n*, *m* representing the initial reacting mass of C_3N_4-rGO-*x* in mg, *n* representing that of $Na_2WO_4 \cdot 2H_2O$. Taking C_3N_4-rGO-150-WO_3 400–260 for example, 400 mg of C_3N_4-rGO-150 and 260 mg of $Na_2WO_4 \cdot 2H_2O$ (99%, Aldrich) were mixed in 30 mL of deionized water and kept under stirring at *ca.* 300 rpm for 12 h. Then the pH value was adjusted to 2 using diluted HCl solution. After further stirring at *ca.* 300 rpm for another 12 h, the suspension was transferred into a Teflon-lined steel autoclave and kept at 160 °C for 18 h. The C_3N_4-WO_3 composite was obtained by the same method except for using pure C_3N_4 instead of C_3N_4-rGO composites. After hydrothermal reaction, the resulted composites were separated by centrifugation at 4000 rpm and washed with distilled water several times before drying at 90 °C for 3 h.

Pt-loading on the C_3N_4-rGO, C_3N_4-rGO-WO_3 and C_3N_4-WO_3 composites

Pt was firstly loaded onto the specimen by impregnation: an appropriate amount of H_2PtCl_6 solution (*ca.* 4 mL) was impregnated into the sample powders by evaporating the solvent of the mixed suspension at 90 °C until dry. For the H_2-evolution test by C_3N_4-rGO composites, these Pt-loaded samples were used in the presence of triethanolamine (TEOA) as sacrificial agent. For the overall water splitting test by C_3N_4-rGO-WO_3 and C_3N_4-WO_3 composites, these Pt-loaded samples were further reduced by $NaBH_4$ solution in Ar protection. For example, 200 mg of C_3N_4-rGO-150-WO_3 400–260 loaded with 1 wt% Pt was dissolved in 30 mL of deionized water and purged with Ar for 30 min before adding 5 mg of $NaBH_4$. After 2 h of reduction, the suspension was centrifuged and washed with distilled water several times. The resulted slurry was then used for photocatalytic tests.

Material characterization

Specimens were characterized by XRD using a PANalytical Empyrean Reflection diffractometer with a Cu Kα source (λ = 1.541 Å). TEM analysis was performed using a JEM-2011. XPS spectra were obtained using an ESCALAB 250 and all binding energies were referenced to the C 1s peak at 284.6 eV. A UV–vis spectrophotometer (JASCO-V550) was used for obtaining the optical absorbance spectra.

Photocatalytic measurement

The measurement was performed with a home-made Teflon reactor with the top window sealed by Pyrex glass. In the H_2-evolution test by C_3N_4-rGO composites loaded with 1 wt% Pt, 200 mg of photocatalyst was dispersed in 100 mL of water and 10 mL of TEOA was added as sacrificial agent. In the O_2-evolution test by $WO_3 \cdot 1/3H_2O$, 100 mg of $WO_3 \cdot 1/3H_2O$

powder was dispersed in 100 mL of water with 10 mmol L^{-1} $AgNO_3$ as an electron acceptor. The reactor was firstly purged with pure Ar to remove air from the reaction system, then the solution was irradiated by a 250 W iron doped metal halide UV–vis lamp (UV Light Technology Limited, UK) with a UV cut-off filter ($\lambda > 420$ nm) and the amount of H_2 or O_2 produced was determined by gas chromatography (Agilent 3000 Micro Gas Chromatograph with a TCD detector, using argon carrier gas). The H_2- and O_2-evolution half reaction results shown in the ESI† demonstrated their activity under visible light. The mediator-free Z-scheme overall water splitting reaction trials were performed in the same top-irradiation system. During these trials, 200 mg of Pt-loaded C_3N_4-rGO-WO_3 or C_3N_4-WO_3 composites was suspended in 100 mL of deionized water, but no TEOA was added. The evolved gas composition in the sealed reactor was measured by gas chromatography.

Quantum yield efficiency measurement

The apparent quantum yield (AQY) of the Z-scheme water splitting with a two-photon excitation process was measured using the same reactor with the addition of a band-pass filter (420 nm, $\Delta\lambda_{1/2}$ = 10 nm). The AQY values were calculated using the following equation:[22]

$$\text{AQY}\ (\%) = [4 \times n(H_2)]/n(\text{photons}) \times 100 \quad (1)$$

where $n(H_2)$ and n(photons) represent the quantities of evolved H_2 molecules and the number of incident photons, respectively. The total number of incident photons was determined using a grating spectroradiometer (Apogee Instruments, Inc, Model MQ-200) and the the incident photon power in the apparent quantum yield measurement is about 120 μmol m^{-2} s^{-1}.

3. Results and discussion

Fig. 1 shows the typical XRD patterns of WO_3 and C_3N_4-rGO-150-WO_3 composites resulting from the hydrothermal reaction of $Na_2WO_4{\cdot}2H_2O$ without or with different contents of C_3N_4-rGO-150. The XRD pattern in Fig. 1a denotes the presence of orthorhombic tungsten oxide one third hydrate ($WO_3{\cdot}1/3H_2O$, JCPDS card no. 54-1012), and the characteristic peak from C_3N_4 located at around 27° increased with the increment of C_3N_4-rGO-150 content, as shown in Fig. 1b and c. There are no obvious diffraction peaks for $WO_3{\cdot}1/3H_2O$ in Fig. 1c, which may be due to the large molar ratio of C_3N_4 to WO_3 in C_3N_4-rGO-150-WO_3 1000–260 (*ca.* 13.8 calculated from the added amount). If considering the smaller density and bigger particle size of C_3N_4 than WO_3 nanoparticles in C_3N_4-rGO-150-WO_3 1000–260, the XRD diffraction density of C_3N_4 is much stronger than that of WO_3 nanoparticles. Therefore, the diffraction peaks of $WO_3{\cdot}1/3H_2O$ properly overlapped with those of C_3N_4. In addition, the crystallinity of WO_3 may be also poor because of the dispersion of C_3N_4 particles.

Fig. 2a and b show the TEM images of C_3N_4-rGO-150-WO_3 400–260 and C_3N_4-rGO-150-WO_3 1000–260, respectively. It is obvious that in the hydrothermal reaction, a higher $Na_2WO_4{\cdot}2H_2O$/C_3N_4-rGO-150 ratio means that more isolated WO_3 particles are not loaded on the surface of C_3N_4-rGO-150, while in C_3N_4-rGO-150 1000–260, almost no independent WO_3 particles exist. By loading Pt as co-catalyst, efficient H_2-evolution performance can be realized. Fig. 2c and S1 (see in ESI†) show the TEM images of C_3N_4-rGO-150 400–260 loaded with 1 wt% Pt after several periods of photocatalytic water splitting tests, indicating that Pt is mainly distributed onto the surface of C_3N_4 perhaps due to its stronger ability to chelate Pt^+. The typical UV–vis light absorbance spectra in Fig. 2d also indicate that there were no obvious differences in the

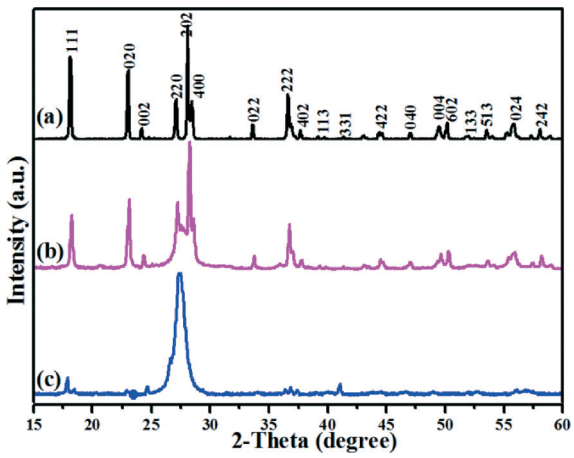

Fig. 1 XRD patterns of pure WO_3 (a), C_3N_4-rGO-150-WO_3 400–260 (b) and C_3N_4-rGO-150-WO_3 1000–260 (c).

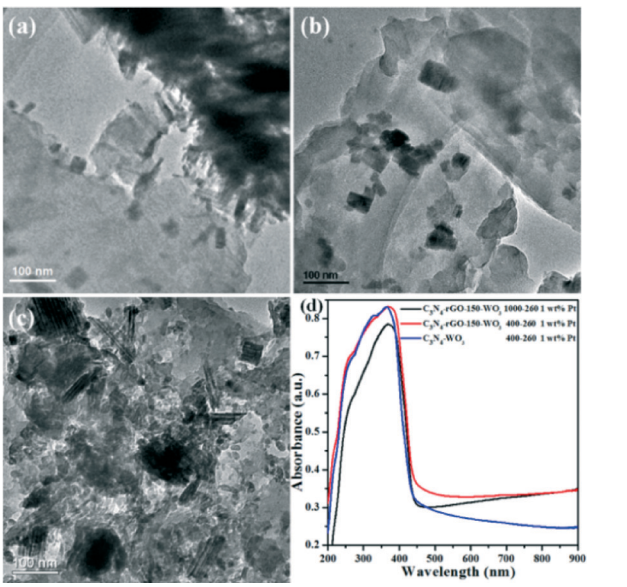

Fig. 2 TEM images of C_3N_4-rGO-150-WO_3 400–260 (a), C_3N_4-rGO-150-WO_3 1000–260 (b), C_3N_4-rGO-150-WO_3 400–260 loaded with 1 wt% Pt after photocatalytic test (c); the UV–vis light absorbance spectra (converted from the corresponding reflectance spectra) of three typical samples loaded with 1 wt% Pt (d).

absorbance between the composites with different WO_3 contents, while adding rGO indeed increased the absorption toward visible light.

We used the as-prepared C_3N_4-rGO-150-WO_3 400–260 without loading Pt as photocatalyst for the cycling water-splitting test under visible light (Fig. 3). As shown in Fig. 3a, in the initial four cycles, the performance increased but then decayed on further cycling. The best performance is only about 12 μmol of H_2 in 20 hours' irradiation. After loading Pt as co-catalyst, the case is much different, as shown in Fig. 3b. The H_2-evolution performance is very stable from the second cycle and the final amount of H_2 produced in 20 hours is as high as 35 μmol and the produced O_2 is about half in μmol compared with that of H_2. It is also noted that without loaded Pt, the photocatalyst underwent an obvious color change during the photo-reaction as shown in Fig. 3c and d, where the milk-white suspension changed into blue after six cycles of test. According to much reported research on the photochromogenic WO_3, when irradiated at a photo energy higher than its band gap (2.8 eV), photochromism would occur, in which the photo-generated electron–hole would lead to the reduction of W^{6+} into blue-colored W^{5+}.[23–28] While after being loaded with Pt nanoparticles, the photocatalyst became just a little darker compared with that of the milk-white C_3N_4-rGO-150-WO_3 400–260, and no color change occurred during the photo-reaction, as shown in Fig. 3e. It was discovered that the loaded Pt was able to inhibit the color change, which may be due to the efficient electron capture by the loaded Pt nanoparticles. The gas generation amount dependence on reaction time shown in Fig. S2† for C_3N_4-rGO-150-WO_3 400–260 loaded with 1 wt% Pt indicates

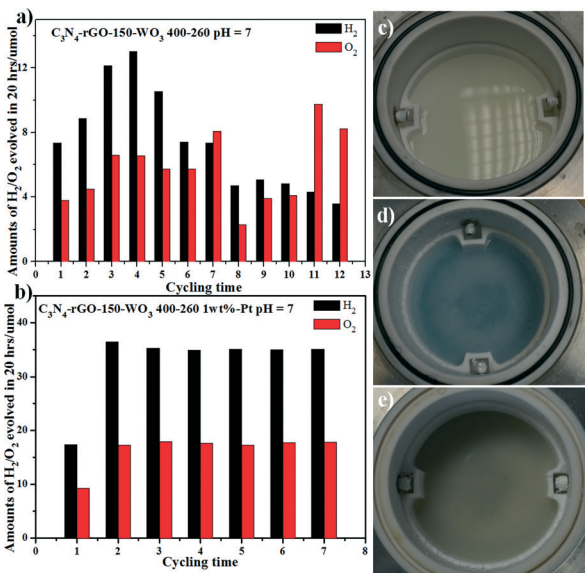

Fig. 3 The performance of the cycling test for C_3N_4-rGO-150-WO_3 400–260 without (a) and with (b) Pt under pH = 7; the C_3N_4-rGO-150-WO_3 400–260 without Pt before photo-reaction (c) and after six cycles of photo-reaction (d); the sample C_3N_4-rGO-150-WO_3 400–260 with Pt after six cycles of photo-reaction (e).

that gaseous products evolve linearly for the next 12 h in a ratio of *ca.* 2 : 1 (H_2 and O_2: 1.52 and 0.74 μmol h^{-1}) under visible light.

To investigate the effects of graphene content, the mass ratio of C_3N_4 (or C_3N_4/rGO) and WO_3, the pH in the photocatalytic system and the amount of loaded Pt on the water-splitting performance, we tested the H_2/O_2 evolution amount with different photocatalysts and in different conditions. As indicated by no. 1 and 2 in Table 1, when using only C_3N_4 loaded with 1 wt% Pt in nonsacrificial conditions, no water splitting occurred, while when using C_3N_4-rGO-150 composite loaded with 1 wt% Pt, the produced H_2 is about 3.3 μmol in 20 hours' irradiation. In Jorge *et al.*'s work, C_3N_4 was used for H_2 and O_2 evolution from water half-splitting with methanol and Ag^+ as sacrificial agent, respectively.[29] In our photocatalytic reaction test, no. 2, the little water splitting activity should come from the reduction and oxidation of water due to the improved electron–hole separation by graphene. In no. 3–6, it is also shown that different rGO contents in the C_3N_4-rGO composites have a great effect on the water-splitting activity. Both no rGO and too much rGO in the C_3N_4-rGO composites give worse performance for the H_2/O_2 evolution than that in the C_3N_4-rGO-150 composite (no. 3), even though the C_3N_4-rGO-150 composite only displays an enhancement of 15.8% for the H_2/O_2 evolution over the pure C_3N_4 and WO_3 system (no. 6). We have also investigated the rGO effect by testing the H_2-evolution performance using different C_3N_4-rGO composites with TEOA as sacrificial agent and Pt as co-catalyst (more details in Fig. S3 and Table S1 in ESI†). It is implied that rGO has two synergistic effects, one is to prevent the hole–electron recombination by transferring electrons, and the other is to prevent the efficient irradiation due to its opacity and light scattering.[30–32] An appropriate amount of graphene in the C_3N_4-rGO composite would improve the electron transfer and further prevent the charge carrier-recombination,[33–35] thus a little enhancement occurred for C_3N_4-rGO-150 composite with Pt as co-catalyst.

The results for no. 3 and 8 in Table 1 show that sample C_3N_4-rGO-150-WO_3 1000–260 displays a higher performance by 37% than C_3N_4-rGO-150-WO_3 400–260 under the same conditions (*i.e.*, loaded with 1 wt% Pt in pH = 7), indicating that too much WO_3 deposited on the surface of C_3N_4-rGO-150 will prevent the incident light from reaching the C_3N_4-rGO-150 surface, which results in the weakened photoexcitation of C_3N_4-rGO-150.[36] However, for the pure C_3N_4 and WO_3 system, there is no obvious change in the water-splitting performance with different mass ratios of C_3N_4 to WO_3 (no. 6 and 7 in Table 1). These results show that the WO_3 amount has a more obvious influence on the C_3N_4-rGO-150 system than the pure C_3N_4 system, further suggesting that rGO is able to play a significant role in the Z-scheme water-splitting system because of its good conductivity and its function as promising electron mediator for transferring the photo-generated electrons from WO_3 to the photo-generated holes in C_3N_4. The effect of the loaded Pt amount is also revealed from a comparison between no. 5 and 9 or no. 3 and 10. Too

Table 1 Overall water splitting under visible light by C_3N_4-WO_3 system in the presence and absence of rGO[a]

No.	Hydrothermal conditions			Amount of loaded Pt[b]	pH[c]	Activity after 20 h irradiation	
	Type of C_3N_4 or C_3N_4-rGO	C_3N_4 or C_3N_4-rGO (mg)	$Na_2WO_4{\cdot}2H_2O$ (mg)			H_2 (μmol)	O_2 (μmol)
1	Pure C_3N_4	400	0	1 wt% Pt	7	Trace	Trace
2	C_3N_4-rGO-150	400	0	1 wt% Pt	7	3.3	1.1
3	C_3N_4-rGO-150	400	260	1 wt% Pt	7	35.1	18.5
4	C_3N_4-rGO-80	400	260	1 wt% Pt	7	26.1	14.1
5	C_3N_4-rGO-50	400	260	1 wt% Pt	7	20.8	11.2
6	Pure C_3N_4	400	260	1 wt% Pt	7	30.3	14.8
7	Pure C_3N_4	1000	260	1 wt% Pt	7	29.9	14.5
8	C_3N_4-rGO-150	1000	260	1 wt% Pt	7	48.1	24.5
9	C_3N_4-rGO-50	400	260	3 wt% Pt	7	6.0	3.3
10	C_3N_4-rGO-150	400	260	3 wt% Pt	7	11.0	5.0
11	C_3N_4-rGO-150	1000	260	1 wt% Pt	3	11.4	30.5
12	C_3N_4-rGO-150	1000	260	1 wt% Pt	5	29.0	15.1
13	C_3N_4-rGO-150	1000	260	1 wt% Pt	8	53.5	26.8
14	C_3N_4-rGO-150	1000	260	1 wt% Pt	10	56.6	29.2

[a] Conditions: photocatalyst (200 mg in total) in water (100 mL); light source, 250 W iron-doped metal halide ultraviolet–visible lamp, with a cut-off filter ($\lambda > 420$ nm); top-irradiation cell with a quartz glass. [b] Pt was loaded firstly by impregnation of H_2PtCl_6, then lateral reduction with $NaBH_4$ solution and lastly washing several times before using as photocatalyst in slurry. [c] The pH of the suspension in the photocatalystic test system.

much Pt has a negative effect on the gas evolution, as proved by other reports.[37–39]

According to previous research on the Z-scheme photocatalyst system, to ensure the charge transfer, intimate physical interaction between the two photocatalysts was often realized by the aggregation of the two photocatalysts under some appropriate pH.[8,11] In our case, the effect of pH on the water-splitting activity was also investigated using C_3N_4-rGO-150-WO_3 1000–260 as target. It is found that with increasing pH, the gas evolution rate is gradually increased (no. 8, 11–14). When the pH equals 3, the produced H_2 is as low as 11.4 μmol in 20 hours. Since WO_3 is inherently unstable at high pH, we did not test the performance under higher pH conditions. Thus the pH effect should not come from the aggregation level but from the kinetic rate of the H_2 and O_2 evolution reactions, which can be expressed as the following:

$$2H^+ + 2e^- \rightarrow H_2 \quad (2)$$

$$2H_2O + 4h^+ \rightarrow O_2 + 4H^+ \quad (3)$$

It can be inferred that although pH has the conflicting effect for eqn (2) and (3), a higher pH is beneficial to the whole performance. This is despite that under acidic conditions, H_2-evolution reaction is relatively favorable, the associated negative effect for the O_2 evolution would trade off the little benefit since the water oxidation depends on the adsorbed OH^- ions onto the WO_3 surface and their following oxidation by multiple photo-generated holes.[40] Thus under more alkaline conditions, the final H_2/O_2-evolution performance turns out to be higher, and these results indicate that the O_2-evolution reaction is the rate-determining process.

We also prepared a C_3N_4-WO_3 composite *via* two other methods, one by calcining WO_3 nanoparticles and C_3N_4 mixture at 350 °C and the other by hydrothermal treatment of WO_3 nanoparticles and C_3N_4 mixture at 160 °C. Both of the as-prepared mixtures were loaded with 1 wt% Pt before the photocatalytic test. And for the two cases, no H_2 was detected. It is confirmed that the hydrothermal conditions result in the intimate contact between C_3N_4 (or C_3N_4-rGO) and WO_3 due to the special high-temperature and high-pressure environment. And the *in situ* formation of WO_3 particles on the C_3N_4 framework also contributes to the intimate interaction between the two photocatalysts.

It is worthy to note that the photocatalysts used in Table 1 were fresh wet samples from the reduction by $NaBH_4$ without drying. And we also tried to dry the sample C_3N_4-rGO-150-WO_3 1000–260 (loaded with 1 wt% Pt) after several cycling tests with stable performance. Interestingly, after drying in air at 80 °C for 4 hours, the sample showed a lower activity than its stable performance before drying, and only after 3 cycles, was the performance recovered, as shown in Fig. 4. Then the sample was dried again at 80 °C for 30 hours, after which the H_2/O_2 evolution became even worse, and also recovered after 4 cycles (Fig. 4a). We investigated the XPS of the sample dried in air at 80 °C for 30 hours and the fresh wet sample dried in Ar. The XPS survey spectrum shown in Fig. S4 (see in ESI†) demonstrated the existence of C, N, O, Pt and W, but no Na was observed. Although both of the samples showed a high content of PtO_x (indicated by the Pt $4f_{7/2}$ and Pt $4f_{5/2}$ peaks centered at *ca.* 73.0 eV and 76.3 eV, respectively),[41] the metallic Pt content in the sample dried in Ar is obviously higher than that dried in air (indicated by the Pt $4f_{7/2}$ and Pt $4f_{5/2}$ peaks centered at *ca.* 71.0 eV and 74.3 eV, respectively), as shown in Fig. 4b and c.[42] Therefore, it is inferred that the evolved H_2 would reduce PtO_x into Pt metal during the irradiation and the activity of the sample is quite sensitive to the Pt metal content.

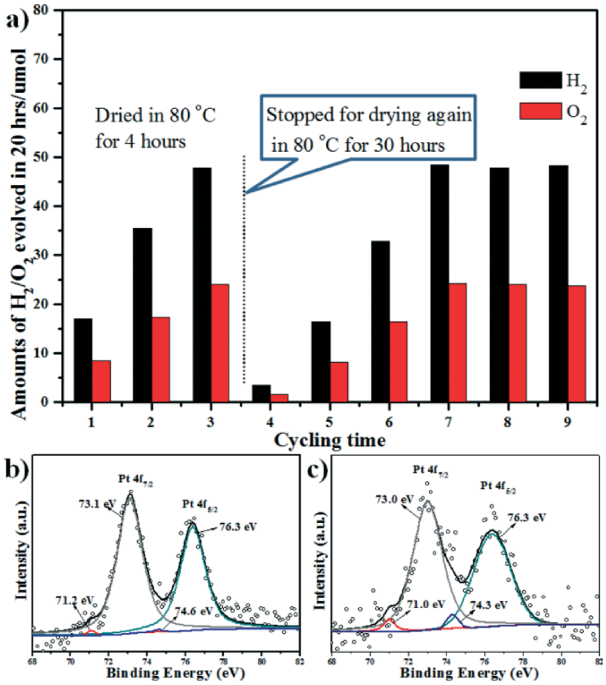

Fig. 4 The cycling performance of the sample (C_3N_4-rGO-150-WO_3 1000–260 loaded with 1 wt% Pt) dried after several photo-test cycles as fresh slurry (a); XPS of the sample dried in air for 30 hours (b); XPS of the fresh wet sample dried in Ar (c).

The evolution of H_2 from water splitting was further confirmed by using D_2O as the solvent in the suspension of photocatalyst. The evolved gas mixture was then detected by the mass spectra and the results are shown in Fig. S5 (see in ESI†). The extra signal located at 4 amu is due to evolved D_2, which is absent in that of the background gas. We also measured the apparent quantum yield efficiency under monochromatic light at 420 nm. The sample C_3N_4-rGO-150-WO_3 1000–260 (loaded with 1 wt% Pt) under neutral conditions shows an AQY efficiency of *ca.* 0.9% while the homologous sample without rGO shows a smaller value (*i.e.*, 0.7%), further demonstrating the positive effect of rGO.

Although Martin *et al.*[10] recently reported a similar Z-scheme water splitting on the basis of C_3N_4 and WO_3 (or $BiVO_4$), their performance is strongly dependent on the redox mediator type (*i.e.*, I^-/IO_3^-) and the pH. However, in our C_3N_4-rGO (or C_3N_4) and WO_3 composite system, no redox mediator is needed for the water-splitting photocatalytic test, which further infers that the intimate contact resulting from hydrothermal conditions is of benefit to the H_2/O_2 evolution in the two-step photoexcitation *Z*-scheme system. Fig. 5 shows a tentatively proposed mechanism for the H_2/O_2 evolution by the C_3N_4-WO_3 composite with or without the mediation of rGO. According to a previous study, the CB and VB positions of WO_3 are located at about +0.41 eV and +3.18 eV,[43] while those of C_3N_4 are about −1.13 eV and +1.57 eV.[19] It is not difficult to infer that under irradiation, O_2 could be evolved from the WO_3 surface and H_2 from the C_3N_4 surface.

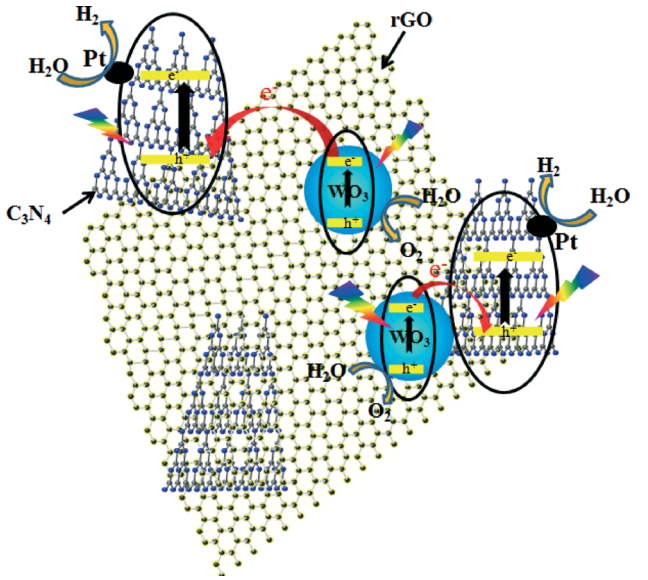

Fig. 5 Proposed mechanism for the H_2/O_2 evolution by C_3N_4-WO_3 composite with or without the mediation of rGO.

Considering the Pt function as discussed above, H_2 is more readily evolved from the surface of Pt than that of C_3N_4. Therefore, water is oxidized by the photo-induced holes in the VB of WO_3 and reduced by the electrons on Pt trapped from the CB of C_3N_4. The electrons on CB of WO_3 are able to combine with the holes in VB of C_3N_4 at the interface due to the intimate contact. rGO successfully functions as a positive electron mediator because of its good conductivity for electron migration, its sturdy contact with C_3N_4 resulted from its calcination with the precursor (*i.e.*, melamine), and its good contact with WO_3 particles under the hydrothermal conditions.

4. Conclusions

In summary, we have introduced a mediator-free Z-scheme system design based on C_3N_4 by utilizing WO_3 as O_2 photocatalyst for the first time, where C_3N_4 and WO_3 are combined as composites through a facile hydrothermal method. Successful water splitting under visible light ($\lambda > 420$ nm) can be realized without any redox mediator when Pt is loaded on the surface of the composites. More importantly, rGO is introduced into these composites to form C_3N_4-rGO-WO_3 composites and this shows a positive effect on the performance in an optimized amount. The highest H_2/O_2 evolution rates are about 2.84 and 1.46 μmol h^{-1} under visible light ($\lambda > 420$ nm) with a quantum yield of 0.9% at 420 nm. Although the resulting performance is not in the highest for water splitting, the newly proposed methodology for constructing heterostructures through the hydrothermal method will pave the way for more efficient overall water splitting with two-step photoexcitation Z-scheme systems in the absence of a redox mediator.

Acknowledgements

The authors gratefully thank the Engineering and Physical Sciences Research Council (EPSRC) platform grant EP/K006800/1, EP/K036769/1 and EP/K022237/1 for financial support.

Notes and references

1 N. S. Lewis, *Science*, 2007, **315**, 798–801.
2 R. Abe, T. Takata, H. Sugihara and K. Domen, *Chem. Commun.*, 2005, 3829–3831.
3 M. Tabata, K. Maeda, M. Higashi, D. Lu, T. Takata, R. Abe and K. Domen, *Langmuir*, 2010, **26**, 9161–9165.
4 H. Kato, M. Hori, R. Konta, Y. Shimodaira and A. Kudo, *Chem. Lett.*, 2004, **33**, 1348–1349.
5 R. M. Navarro, M. C. Alvarez-Galvan, J. A. Villoria de la Mano, S. M. Al-Zahrani and J. L. G. Fierro, *Energy Environ. Sci.*, 2010, **3**, 1865–1882.
6 S. J. A. Moniz, S. A. Shevlin, D. J. Martin, Z.-X. Guo and J. Tang, *Energy Environ. Sci.*, 2015, **8**, 731–759.
7 Y. Miseki, S. Fujiyoshi, T. Gunji and K. Sayama, *Catal. Sci. Technol.*, 2013, **3**, 1750–1756.
8 Y. Sasaki, H. Nemoto, K. Saito and A. Kudo, *J. Phys. Chem. C*, 2009, **113**, 17536–17542.
9 M. Higashi, R. Abe, K. Teramura, T. Takata, B. Ohtani and K. Domen, *Chem. Phys. Lett.*, 2008, **452**, 120–123.
10 D. J. Martin, P. J. T. Reardon, S. J. A. Moniz and J. Tang, *J. Am. Chem. Soc.*, 2014, **136**, 12568–12571.
11 A. Iwase, Y. H. Ng, Y. Ishiguro, A. Kudo and R. Amal, *J. Am. Chem. Soc.*, 2011, **133**, 11054–11057.
12 K. Yamaguti and S. Sato, *J. Chem. Soc., Faraday Trans. 1*, 1985, **81**, 1237–1246.
13 K. Maeda, K. Teramura, D. Lu, N. Saito, Y. Inoue and K. Domen, *Angew. Chem., Int. Ed.*, 2006, **45**, 7806–7809.
14 F. Goettmann, A. Fischer, M. Antonietti and A. Thomas, *Angew. Chem., Int. Ed.*, 2006, **45**, 4467–4471.
15 F. Goettmann, A. Fischer, M. Antonietti and A. Thomas, *Chem. Commun.*, 2006, 4530–4532.
16 X. Wang, K. Maeda, A. Thomas, K. Takanabe, G. Xin, J. M. Carlsson, K. Domen and M. Antonietti, *Nat. Mater.*, 2009, **8**, 76–80.
17 X. Wang, K. Maeda, X. Chen, K. Takanabe, K. Domen, Y. Hou, X. Fu and M. Antonietti, *J. Am. Chem. Soc.*, 2009, **131**, 1680–1681.
18 Z. Zhao, Y. Sun and F. Dong, *Nanoscale*, 2015, **7**, 15–37.
19 S. C. Yan, S. B. Lv, Z. S. Li and Z. G. Zou, *Dalton Trans.*, 2010, **39**, 1488–1491.
20 H. Kominami, K.-i. Yabutani, T. Yamamoto, Y. Kera and B. Ohtani, *J. Mater. Chem.*, 2001, **11**, 3222–3227.
21 G. Zhao, J. Li, X. Ren, C. Chen and X. Wang, *Environ. Sci. Technol.*, 2011, **45**, 10454–10462.
22 Q. Wang, T. Hisatomi, S. S. K. Ma, Y. Li and K. Domen, *Chem. Mater.*, 2014, **26**, 4144–4150.
23 C. Bechinger, G. Oefinger, S. Herminghaus and P. Leiderer, *J. Appl. Phys.*, 1993, **74**, 4527–4533.
24 J. G. Zhang, D. K. Benson, C. E. Tracy, S. K. Deb, A. W. Czanderna and C. Bechinger, *J. Electrochem. Soc.*, 1997, **144**, 2022–2026.
25 Y. He, Z. Wu, L. Fu, C. Li, Y. Miao, L. Cao, H. Fan and B. Zou, *Chem. Mater.*, 2003, **15**, 4039–4045.
26 W. Morales, M. Cason, O. Aina, N. R. de Tacconi and K. Rajeshwar, *J. Am. Chem. Soc.*, 2008, **130**, 6318–6319.
27 G. Hodes, D. Cahen and J. Manassen, *Nature*, 1976, **260**, 312–313.
28 M. A. Butler, R. D. Nasby and R. K. Quinn, *Solid State Commun.*, 1976, **19**, 1011–1014.
29 A. B. Jorge, D. J. Martin, M. T. S. Dhanoa, A. S. Rahman, N. Makwana, J. Tang, A. Sella, F. Corà, S. Firth, J. A. Darr and P. F. McMillan, *J. Phys. Chem. C*, 2013, **117**, 7178–7185.
30 W. Ho, J. C. Yu, J. Lin, J. Yu and P. Li, *Langmuir*, 2004, **20**, 5865–5869.
31 J. Yu, Y. Hai and M. Jaroniec, *J. Colloid Interface Sci.*, 2011, **357**, 223–228.
32 J. Yu, X. Zhao and Q. Zhao, *Thin Solid Films*, 2000, **379**, 7–14.
33 X.-H. Li, J.-S. Chen, X. Wang, J. Sun and M. Antonietti, *J. Am. Chem. Soc.*, 2011, **133**, 8074–8077.
34 Q. Xiang, J. Yu and M. Jaroniec, *J. Phys. Chem. C*, 2011, **115**, 7355–7363.
35 Y. Li, H. Zhang, P. Liu, D. Wang, Y. Li and H. Zhao, *Small*, 2013, **9**, 3336–3344.
36 P. Zhou, J. Yu and M. Jaroniec, *Adv. Mater.*, 2014, **26**, 4920–4935.
37 M. Hara, J. Nunoshige, T. Takata, J. N. Kondo and K. Domen, *Chem. Commun.*, 2003, 3000–3001.
38 N. Bao, L. Shen, T. Takata and K. Domen, *Chem. Mater.*, 2007, **20**, 110–117.
39 K. Maeda, X. Wang, Y. Nishihara, D. Lu, M. Antonietti and K. Domen, *J. Phys. Chem. C*, 2009, **113**, 4940–4947.
40 Y. Zhong, K. Ueno, Y. Mori, X. Shi, T. Oshikiri, K. Murakoshi, H. Inoue and H. Misawa, *Angew. Chem.*, 2014, **126**, 10518–10522.
41 G. M. Bancroft, I. Adams, L. L. Coatsworth, C. D. Bennewitz, J. D. Brown and W. D. Westwood, *Anal. Chem.*, 1975, **47**, 586–588.
42 G. Johansson, J. Hedman, A. Berndtsson, M. Klasson and R. Nilsson, *J. Electron Spectrosc. Relat. Phenom.*, 1973, **2**, 295–317.
43 S. J. Hong, S. Lee, J. S. Jang and J. S. Lee, *Energy Environ. Sci.*, 2011, **4**, 1781–1787.

